Unbalance Control of Active Magnetic Bearings

Beat Aeschlimann*, Michael Hubatka*

* Mecos AG, Industriestrasse 26, 8404 Winterthur, Switzerland, beat.aeschlimann@mecos.com

***Abstract*—Unbalance forces are a major source of undesired vibrations in rotating machinery. Active magnetic bearings (AMBs) with special control algorithms, allow for controlling those forces and counteract appropriately. The two basic principles are UFRC and UFCC. They are known for many years and have been published and patented before. There exist excellent publications treating the closed-loop stability of UFRC but not much can be found on the stability of UFCC.**

This paper presents an adaptive multi-variable implementation of UFCC, its theoretical background and a proof of control stability. UFCC as described in this paper, has shown excellent stability in practice and it can therefore be engaged over the entire speed range of the machine. However in order to minimize the load on power amplifiers and other components a switching strategy is advised, where UFRC and UFCC are switched on and off in the speed ranges where required. Guidelines for tuning UFCC parameter are also given.

The effectiveness of UFCC has been proven in several applications and measurement results are given in this paper.

I. Introduction

Active Magnetic Bearings (AMB) have some unique features unknown in conventional bearing technologies: Active control of the electromagnetic forces allows setting the bearing properties by the control system. At some point the bearings must provide high stiffness to minimize rotor orbit. But for crossing critical speeds of the rotor, damping is required. State of the art AMB systems feature digital control and the bearing parameter can be adjusted over the entire speed range according to the requirements of machine and process.

Unbalance forces are a major source of undesired vibrations in rotating machinery. They can lead to large shaft orbits or can saturate the power amplifiers. To overcome these problems special control strategies have been developed during the last decades, such as UFRC and UFCC [1].

Unbalance force rejection control (UFRC) removes synchronous components from the AMB sensor signals, resulting in force-free operation [2]. To achieve this, either a tracking notch filter is inserted into the feedback loop or a synchronous compensation signal is injected into the loop, matching amplitude and phase of the unbalance disturbance [3]. The second approach has several advantages with regards to stability and robustness [4] and [5]. An new proof of stability and tuning guidelines for this type of UFRC will be presented in a paper at this conference [6].

When the shaft of a turbo machine is operated close to or in a critical speed, the magnitude of shaft deflection may become very large. Unbalance force counteracting control (UFCC) aims at minimizing the synchronous displacement. Typically a compensation signal is injected into the loop at the output of the feedback controller. Amplitude and phase of the compensation signal determine stiffness and damping of UFCC. In [7] and [8] UFCC with signal injection at the output of the feedback controller is used. Positive damping is achieved by derivation of the sensor signal. [9] uses x-y cross-coupling instead of derivatives to introduce damping. In [10] a combination of UFRC and UFCC, balanced by so-called gain controllers is introduced. Suitable choices of phase lead and gain are discussed. [11] proposes a simultaneous compensation of sensor runout and mass unbalance by using bias current excitation. The authors propose Lyapunov based adaptation of the unknown Fourier parameter.

UFRC and UFCC are often designated as 'filters' although this expression is oversimplifying. Other expressions for UFCC are synchronous damping control (SDC) or optimum damping control (ODC) [1].

All mentioned implementations of UFCC have in common, that the closed-loop stability is affected. Unfortunately not all mentioned publications include stability considerations. This paper presents an implementation of a combined UFRC/UFCC in Chapter II and a proof of stability in Chapter III. In Chapter IV guidelines for the choice of parameter are given. The stability and effectiveness of UFCC is shown by measurement results in Chapter V.

II. Working Principle

The basic control scheme used in this paper is shown in Figure 1. The feedback controller $\mathbf{K}(s) \in \mathbb{C}^{pxp}$ stabilizes the control plant $\mathbf{P}(s) \in \mathbb{C}^{pxp}$. The influence of the unbalance is modelled with input $\boldsymbol{f_u}(t)$. We define the error signal $\boldsymbol{e}(t) = \boldsymbol{y}(t) - \boldsymbol{c}(t)$ as the input to $\mathbf{N}_f(s)$ which outputs two signals, $\boldsymbol{c}(t)$ and $\boldsymbol{f_c}(t)$. The compensation signal $\boldsymbol{c}(t)$ eliminates the synchronous component from $\boldsymbol{y}(t)$. The signal $\boldsymbol{f_c}(t)$ is the synchronous force to minimize shaft displacement. They are defined as

$$\boldsymbol{c}(t) = \begin{bmatrix} \sin(\Omega t)\mathbf{I} & \cos(\Omega t)\mathbf{I} \end{bmatrix} \begin{bmatrix} \hat{\boldsymbol{x}}_{\mathbf{1}}(t) \\ \hat{\boldsymbol{x}}_{\mathbf{2}}(t) \end{bmatrix} \tag{1}$$

$$\boldsymbol{f_c}(t) = \begin{bmatrix} \sin(\Omega t)\mathbf{I} & \cos(\Omega t)\mathbf{I} \end{bmatrix} \begin{bmatrix} \mathbf{Q} \end{bmatrix} \begin{bmatrix} \hat{\boldsymbol{x}}_{\mathbf{1}}(t) \\ \hat{\boldsymbol{x}}_{\mathbf{2}}(t) \end{bmatrix} \tag{2}$$

where $\mathbf{I}$ is the identity matrix $\mathbf{I}^{pxp}$ and $\hat{\boldsymbol{x}}_{\mathbf{1}}(t)$ and $\hat{\boldsymbol{x}}_{\mathbf{2}}(t)$ $\in \mathbb{R}^{px1}$ are the states of $\mathbf{N}_f(s)$ corresponding to the amplitudes of sine and cosine. The amplitudes are computed by the demodulator $\mathbf{DM}$ as described in [5].

The feed-forward matrix $\mathbf{Q} \in \mathbb{R}^{2px2p}$ determines gain and phase of $\boldsymbol{f_c}$ with regards to $\boldsymbol{c}$. Since it is a full matrix any linear combinations of the elements of $\hat{\boldsymbol{x}}_{\boldsymbol{1}}(t)$ and $\hat{\boldsymbol{x}}_{\boldsymbol{2}}(t)$ can be formed and thus $\boldsymbol{f_c}$ can have arbitrary phase lead. More details are given in Chapter IV.

III. Stability Proof

To investigate the stability of UFCC the same approach as [6] uses for UFRC is applied here. $\mathbf{N}_f(s)$ is described as an observer for the states $\hat{\boldsymbol{x}}_{\boldsymbol{1}}(t)$ and $\hat{\boldsymbol{x}}_{\boldsymbol{2}}(t)$ with the following state space equations

$$\begin{aligned}\begin{bmatrix}\dot{\hat{\boldsymbol{x}}}_{\boldsymbol{1}}(t)\\ \dot{\hat{\boldsymbol{x}}}_{\boldsymbol{2}}(t)\end{bmatrix} &= \begin{bmatrix}\mathbf{0} & -\Omega\mathbf{I}\\ \Omega\mathbf{I} & \mathbf{0}\end{bmatrix}\begin{bmatrix}\hat{\boldsymbol{x}}_{\boldsymbol{1}}(t)\\ \hat{\boldsymbol{x}}_{\boldsymbol{2}}(t)\end{bmatrix} + \begin{bmatrix}\mathbf{T}_R(\Omega)\\ \mathbf{T}_J(\Omega)\end{bmatrix}\boldsymbol{e}(t)\\ \begin{bmatrix}\boldsymbol{c}(t)\\ \boldsymbol{f_c}(t)\end{bmatrix} &= \begin{bmatrix}\mathbf{I} & \mathbf{0}\\ \mathbf{Q} & \mathbf{0}\end{bmatrix}\begin{bmatrix}\hat{\boldsymbol{x}}_{\boldsymbol{1}}(t)\\ \hat{\boldsymbol{x}}_{\boldsymbol{2}}(t)\end{bmatrix}\end{aligned} \tag{3}$$

Applying the same modal transformation as in [6] to (3) yields the modal state space description with new states $\boldsymbol{m_1}$ and $\boldsymbol{m_2}$

$$\begin{aligned}\begin{bmatrix}\dot{\boldsymbol{m}}_{\boldsymbol{1}}(t)\\ \dot{\boldsymbol{m}}_{\boldsymbol{2}}(t)\end{bmatrix} &= \begin{bmatrix}j\Omega\mathbf{I} & \mathbf{0}\\ \mathbf{0} & -j\Omega\mathbf{I}\end{bmatrix}\begin{bmatrix}\boldsymbol{m_1}(t)\\ \boldsymbol{m_2}(t)\end{bmatrix} + \begin{bmatrix}\mathbf{T}(\Omega)\\ \overline{\mathbf{T}(\Omega)}\end{bmatrix}\boldsymbol{e}(t)\\ \begin{bmatrix}\boldsymbol{c}(t)\\ \boldsymbol{f_c}(t)\end{bmatrix} &= \frac{1}{2}\begin{bmatrix}\mathbf{I} & \mathbf{I}\\ \mathbf{Q} & \mathbf{Q}\end{bmatrix}\begin{bmatrix}\boldsymbol{m_1}(t)\\ \boldsymbol{m_2}(t)\end{bmatrix}\end{aligned} \tag{4}$$

where $\mathbf{T}(\Omega) = \mathbf{T}_R(\Omega) + j\mathbf{T}_J(\Omega)$ and $\overline{\mathbf{T}(\Omega)} = \mathbf{T}_R(\Omega) - j\mathbf{T}_J(\Omega)$ are the observer gains.

When both loops from $\boldsymbol{c}$ and $\boldsymbol{f_c}$ are closed the following two equations hold:

$$\begin{aligned}\boldsymbol{e}(s) &= -\mathbf{S}_e(s)\boldsymbol{c}(s) = -(\mathbf{I} - \mathbf{L}_e(s))^{-1}\boldsymbol{c}(s)\\ \boldsymbol{e}(s) &= -\mathbf{F}_u(s)\boldsymbol{f_c}(s) = -\mathbf{P}(s)(\mathbf{I} - \mathbf{L}_f(s))^{-1}\boldsymbol{f_c}(s)\end{aligned} \tag{5}$$

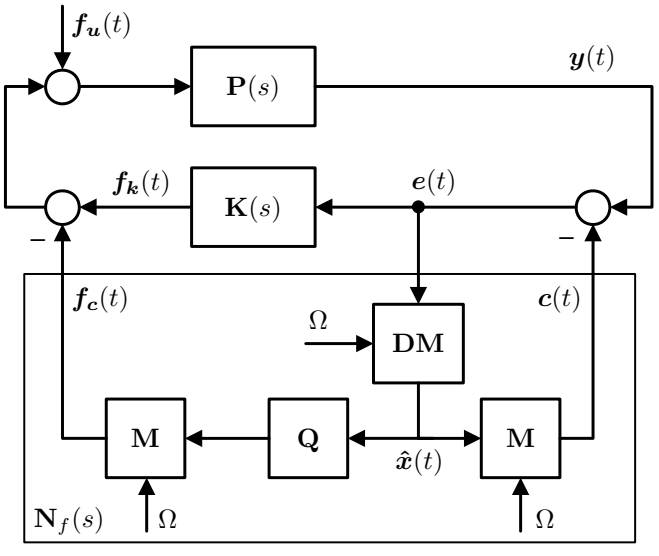

Figure 1. Block diagram of the control system with UFRC and UFCC.

where $\mathbf{S}_e(s)$ is the sensitivity function at loop-breaking point $\boldsymbol{e}$ and $\mathbf{F}_u(s)$ is the dynamic compliance function. $\mathbf{L}_e(s)$ and $\mathbf{L}_f(s)$ are the loop gains at loop-breaking point e and f respectively. The corresponding state-space descriptions are

$$\begin{aligned}\dot{\boldsymbol{x}}_s(t) &= \mathbf{A}_s\boldsymbol{x}_s(t) + \mathbf{B}_s\boldsymbol{c}(t)\\ \boldsymbol{e}(t) &= -\mathbf{C}_s\boldsymbol{x}_s(t) - \mathbf{D}_s\boldsymbol{c}(t)\\ \dot{\boldsymbol{x}}_f(t) &= \mathbf{A}_f\boldsymbol{x}_f(t) + \mathbf{B}_f\boldsymbol{f_c}(t)\\ \boldsymbol{e}(t) &= -\mathbf{C}_f\boldsymbol{x}_f(t) - \mathbf{D}_f\boldsymbol{f_c}(t)\end{aligned} \tag{6}$$

The negative signs in (5) have been included in the output equations. Closing both outer loops yields the closed-loop system matrix

$$\mathbf{A}(\Omega) = \underbrace{\begin{bmatrix}j\Omega\mathbf{I} & \mathbf{0} & \mathbf{0} & \mathbf{0}\\ \mathbf{0} & -j\Omega\mathbf{I} & \mathbf{0} & \mathbf{0}\\ \frac{1}{2}\mathbf{B}_s & \frac{1}{2}\mathbf{B}_s & \mathbf{A}_s & \mathbf{0}\\ \frac{1}{2}\mathbf{B}_f\mathbf{Q} & \frac{1}{2}\mathbf{B}_f\mathbf{Q} & \mathbf{0} & \mathbf{A}_f\end{bmatrix}}_{\mathbf{A}_0(\Omega)} + \underbrace{\begin{bmatrix}-\frac{1}{2}\mathbf{T}(\Omega)\mathbf{D}' & -\frac{1}{2}\mathbf{T}(\Omega)\mathbf{D}' & -\mathbf{T}(\Omega)\mathbf{C}_s & -\mathbf{T}(\Omega)\mathbf{C}_f\\ -\frac{1}{2}\overline{\mathbf{T}(\Omega)}\mathbf{D}' & -\frac{1}{2}\overline{\mathbf{T}(\Omega)}\mathbf{D}' & -\overline{\mathbf{T}(\Omega)}\mathbf{C}_s & -\overline{\mathbf{T}(\Omega)}\mathbf{C}_f\\ \mathbf{0} & \mathbf{0} & \mathbf{0} & \mathbf{0}\\ \mathbf{0} & \mathbf{0} & \mathbf{0} & \mathbf{0}\end{bmatrix}}_{\delta\mathbf{A}(\boldsymbol{\Omega})} \tag{7}$$

with $\mathbf{D}' = (\mathbf{D}_s + \mathbf{D}_f\mathbf{Q})$ and $\mathbf{A}_0(\Omega)$ is the open-loop system matrix with multiple eigenvalues $\pm j\Omega$ and the eigenvalues of $\mathbf{S}_e$ and $\mathbf{F}_u$. Similar to [6] the sensitivity of these eigenvalues $\delta\boldsymbol{\Lambda}(\Omega)$ of $\mathbf{A}(\Omega)$, with respect to $\delta\mathbf{A}(\Omega)$ can be expressed by the right and left eigenvector $\mathbf{U}_0$ and $\mathbf{V}_0^T$ of $\mathbf{A}_0(\Omega)$

$$\delta\boldsymbol{\Lambda}(\Omega) = \operatorname{eig}\left((\mathbf{V}_0^T\mathbf{U}_0)^{-1}\mathbf{V}_0^T\delta\mathbf{A}\mathbf{U}_0\right) \tag{8}$$

It can easily be shown that the following $\mathbf{U}_0$ and $\mathbf{V}_0^T$ are eigenvectors of $\mathbf{A}_0(\Omega)$

$$\mathbf{U}_0 = \begin{bmatrix}\mathbf{I}\\ \mathbf{0}\\ \frac{1}{2}\left(j\Omega\mathbf{I} - \mathbf{A}_s\right)^{-1}\mathbf{B}_s\\ \frac{1}{2}\left(j\Omega\mathbf{I} - \mathbf{A}_f\right)^{-1}\mathbf{B}_f\mathbf{Q}\end{bmatrix} \tag{9}$$

$$\mathbf{V}_0^T = \begin{bmatrix}\mathbf{I} & \mathbf{0} & \mathbf{0} & \mathbf{0}\end{bmatrix} \tag{10}$$

$$\mathbf{V}_0^T\mathbf{U}_0 = \mathbf{I}. \tag{11}$$

and with (8) one gets the solution

$$\begin{aligned}\delta\boldsymbol{\Lambda}(\Omega) = \operatorname{eig}(&-\frac{1}{2}\mathbf{T}(\Omega)(\mathbf{D}_s + \mathbf{D}_f\mathbf{Q})\\ &- \frac{1}{2}\mathbf{T}(\Omega)\mathbf{C}_s(j\Omega\mathbf{I} - \mathbf{A}_s)^{-1}\mathbf{B}_s\\ &- \frac{1}{2}\mathbf{T}(\Omega)\mathbf{C}_f(j\Omega\mathbf{I} - \mathbf{A}_f)^{-1}\mathbf{B}_f\mathbf{Q})\\ = -\frac{1}{2}&\operatorname{eig}\left(\mathbf{T}(\Omega)[\mathbf{S}_e(j\Omega) + \mathbf{F}_u(j\Omega)\mathbf{Q}]\right).\end{aligned} \tag{12}$$

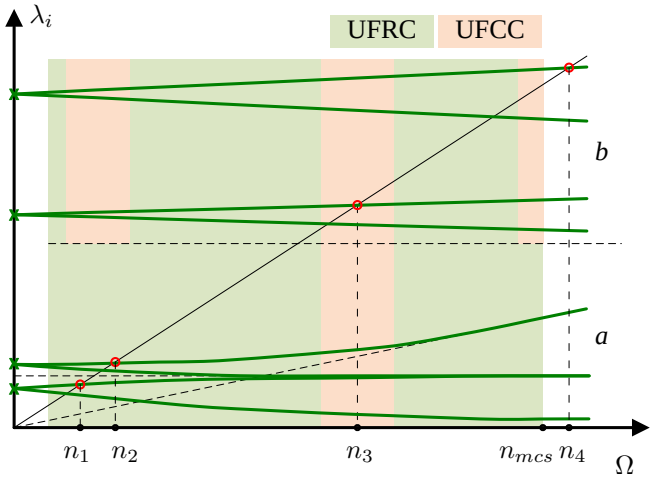

Figure 2. Exemplary Campbell diagram of a turbo machine. λ_i are the shaft eigenfrequencies, n_i are critical speeds of the shaft and n_{mcs} is the maximum continuous speed. The colored areas indicate the speed ranges where UFRC (green) or UFCC (red) are switched on. Pattern *a* is the standard switching pattern, *b* is a more aggressive pattern.

Equation (12) delivers a solution for the closed-loop eigenvalues starting from the open loop eigenvalues $\pm j\Omega$. If all $\delta\mathbf{\Lambda}(\Omega)$ are located in the left half plane then the closed loop is stable. Matrix $\mathbf{T}(\Omega)$ of observer gains is the parameter which ensures closed-loop stability.

IV. Tuning Guidelines

Properly tuned UFCC can be used over the entire speed range of the machine. However in order to minimize bearing current and machine vibration UFCC (and UFRC) are switched on and off depending on rotation speed. Figure 2 shows a Campbell diagram and two different switching patterns for a supercritical shaft. Pattern *a* is the standard pattern: UFCC is switched on only in the vicinity of the 3rd critical speed (first bending). At all other rotation speeds UFRC is engaged and the feedback controller must have sufficient damping. UFCC provides additional damping only for the 3rd critical speed. Alternatively UFRC can be switched on above the the rigid body modes.

If rotor unbalance is large, leading to higher than allowed shaft displacement, then the pattern may be altered: UFCC is additionally switched on around the rigid body modes (1st and 2nd critical speed) to decrease rotor orbits (pattern *b*). At n_{mcs} the shaft is operated close to its 4th critical speed (second bending) where rotor unbalance can also lead to high displacement. If the rotor cannot be balanced then additional damping may be provided by UFCC to counteract. However the effectiveness of UFCC at such high rotation speeds is limited by the bandwidth of the magnetic bearing system.

Based on (12) a straight-forward choice for $\mathbf{T}(\Omega)$ is

$$\mathrm{T}(\Omega) = 2\sigma[\mathbf{S}_e(j\Omega) + \mathbf{F}_u(j\Omega)\mathbf{Q}]^{-1} \tag{13}$$

The sensitivity $\mathbf{S}_e(j\Omega)$ and the compliance $\mathbf{F}_u(j\Omega)$ are computed by using a model of $\mathbf{P}(s)$ according to (5) or can easily be measured on the real system. The (small) number $\sigma \in \mathbb{R}$ defines the convergence speed of UFCC. The higher σ the faster UFCC adapts to a change in $\boldsymbol{f_u}(t)$ which is equivalent to saying, UFCC has high bandwidth. Since $\mathbf{T}(\Omega)$ is not constant and must be loaded e.g. from a look-up table for each speed, also σ can be speed dependent (see: [6]). In general σ must be chosen individually for each application: fast accelerating machines and or flexible shafts typically require larger σ. On the other hand very large σ may deteriorate the robustness of the control loop.

In a machine with asynchronous electric motor, the unbalance magnetic pull modulates unbalance forces with the frequency of electrical slip. In this case σ should be chosen such that the bandwidth of UFCC lies above the slip frequency to compensate for this effect.

The gain and phase of $\boldsymbol{f_c}$ with regards to $\boldsymbol{c}$ is determined by matrix $\mathbf{Q}$. In complex notation $\mathbf{Q}$ can be expressed as $\mathbf{Q}' = |\mathbf{Q}'|\, e^{j\varphi_Q} \in \mathbb{C}^{pxp}$. If φ_Q is set to 0 then $\boldsymbol{f_c}$ is in paraphase to displacement $\boldsymbol{y}$ and corresponds to a stiffness force. If φ_Q is set to $-\pi/2$, then $\boldsymbol{f_c}$ leads $\boldsymbol{y}$ by $\pi/2$ and is a positive damping (note the negative sign of $\boldsymbol{f_c}$ in Figure 1).

An intuitive choice for the magnitude of block diagonal elements Q'_{ii} is

$$|\, Q'_{ii}| = \frac{f_{max,i}}{\delta_{TDB,i}} \left[\frac{N}{m}\right] \tag{14}$$

where $f_{max,i}$ is the maximum force of the radial magnetic bearing i and $\delta_{TDB,i}$ is the touchdown bearing single-sided clearance. Practical experience shows that the gain may be set slightly higher than this. A good start value is (for all bearing planes the same):

$$|\, Q'_{ii}| = 1.4\frac{f_{max,i}}{\delta_{TDB,i}} \left[\frac{N}{m}\right] \tag{15}$$

All off-diagonal elements are set to 0. Note that if $\mathbf{Q}$ is set to $\mathbf{0}$ then (1) corresponds to the UFRC scheme as in [6].

The gain of $\mathbf{Q}$ relates to another issue, which must be taken into account. High gain, combined with high rotor unbalance lead to high forces $\boldsymbol{f_c}$. It must be avoided that $\boldsymbol{f_c}$ saturates the force capacity of the bearings and therefore $\boldsymbol{f_c}$ must be saturated to a predefined value well below the bearing force capacity.

V. Experimental Results

The presented UFCC control has been successfully deployed into several AMB projects of the author's company. In no cases stability problems occurred, also not at very high rotation speeds.

The example given is measurement data from a turbo compressor with four radial bearings and one thrust active magnetic bearing and therefore, an AMB system with nine actively controlled axes. The total rotor length and mass of the machine is approximately 5.5 m and 3 tons. The maximum continuous speed is 166 rps (10000 rpm) and at this speed the machine runs above the 4th critical speed.

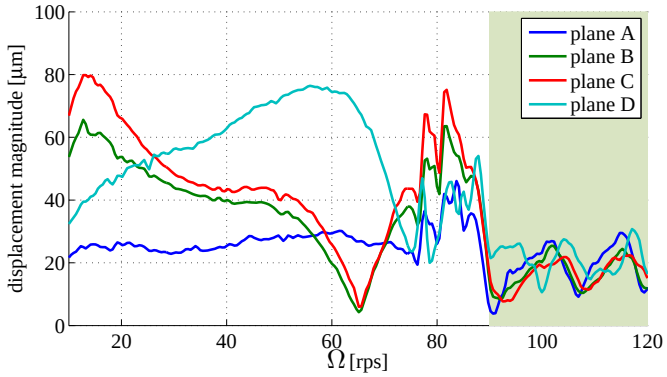

Figure 3. Measured unbalance response of turbo compressor: Only feedback controller up to 90 rps, above UFRC is switched on.

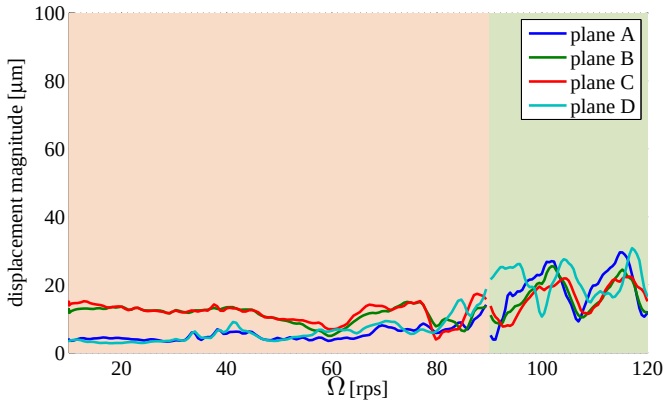

Figure 4. Measured unbalance response of turbo compressor: UFCC is switched on between 10 and 90 rps, above this UFRC is switched on.

In this test the rotor was first accelerated from 0 to n_{mcs} with UFCC switched off and only the feedback controller active. The magnitude of the displacement (0-peak) in each of the four radial bearings was recorded. Then the same measurement was repeated but with UFCC switched on between 10 and 90 rps. This means that UFCC is engaged not only at the 3rd and 4th critical speeds but already well below the rigid body modes. The parameter used are summarized in Table I. The sensitivity function $\mathbf{S}_e(j\Omega)$ and the compliance function $\mathbf{F}_u(j\Omega)$ required to compute $\mathbf{T}(\Omega)$ have been measured by a multi-variable sine sweep method.

The measured unbalance responses of the turbo compressor are shown in Figure 3 and in Figure 4. Without UFCC and only the feedback controller engaged, the shaft displacements reach a maximum value of 80 μm. When UFCC is switched on, the displacements stay well below 20 μm. The effect of UFCC is obvious: Especially the critical speeds responses almost vanish due to the damping provided by UFCC.

VI. Conclusions

A new stability proof for adaptive unbalance force rejection control with signal injection has been presented. A simple equation for the computation of observer gain $\mathbf{T}(\Omega)$ was derived, which is the key for stable operation of UFCC. Guidelines for the choice of UFCC have been given as well.

Table I
UFFC parameter for turbo compressor

Parameter	Value	Unit
σ	0.15	s
$\lvert$ Q'$_{ii}\rvert$	1.4 f$_{max,i}/\delta_{TDB,i} = 100$	N/μm
φ_{Qi}	-$\pi/2$	rad
speed	10...90	rps

This may help the control engineer during commissioning and parameter tuning. Stability and effectiveness of UFCC have been demonstrated with measurement data from a large turbo compressor.

The feed-forward gain $\mathbf{Q}$ has so far been parameterized as block diagonal matrix with no couplings between the bearing planes. Since $\mathbf{S}_e(j\Omega)$ and $\mathbf{F}_u(j\Omega)$ are in general fully coupled it should be investigated if and how additional elements in $\mathbf{Q}$ could further improve the performance of UFCC.

References

[1] *Mechanical Vibration - Vibration of Rotating Machinery Equipped with Active Magnetic Bearings*, ISO Std. 14 839-4.
[2] K. Nonami, Q.-F. Fan, and H. Ueyama, "Unbalance vibration control of magnetic bearing system using adaptive algorithm with disturbance frequency estimation," *Proceedings of the 1999 IEEE International Conference on Control Applications*, 1999.
[3] V. Tamisier, F. Carrere, and S. Font, "Synchronous unbalance cancellation across critical speed using a closed-loop method," *Proceedings of 8th International Symposium on Magnetic Bearings, Mito*, 2002.
[4] R. Larsonneur and R. Herzog, "Feedforward compensation of unbalance: New results and application experiences," *Proceedings of IUTAM Symposium on the Active Control of Vibrations, Bath*, 1994.
[5] R. Herzog, P. Buehler, C. Gaehler, and R. Larsonneur, "Unbalance compensation using generalized notch filters in the multivariable feedback of magnetic bearings," *IEEE Transactions on Control Systems Technology*, vol. 4, no. 5, pp. 580–586, 1996.
[6] M. Hubatka and B. Aeschlimann, "Tuning guidelines for generalized notch filters used for unbalance compensation for magnetic bearings," *Proceedings of 16th International Symposium on Magnetic Bearings, Beijing*, 2018.
[7] H. Habermann and M. Brunet, "The active magnetic bearing enables optimum damping of flexible rotor," *The American Society of Mechanical Engineers*, 1984.
[8] H. Habermann, M. Brunet, and A. Tassel, "Method and device for reducing the vibration of rotating machines equipped with an active magnetic suspension," US Patent 4,626,754, 1986.
[9] O. Matsushita, Takagi, Michiyuki, M. Yoneyama, and T. Sugaya, "Control apparatus for a rotor supported by an electromagnetic bearing," US Patent 4,697,128, 1987.
[10] N. Takahashi, "High-speed rotor and controller for controlling magnetic bearings therefor," US Patent 5,576,587, 1996.
[11] J. D. Setiawan, R. Mukherjee, and E. H. Maslen, "Variable magnetic stiffness approach for simultaneous sensor runout and mass unbalance compensation in active magnetic bearings," *Proceedings of 7th International Symposium on Magnetic Bearings, Zurich*, 2000.